12-21-2016

# Computational Fluid Dynamics Analysis of an Idealized Modern Wingsuit

Maria E. Ferguson
*Washington University in St Louis*

Ramesh K. Agarwal
*Washington University in St. Louis*

# Computational Fluid Dynamics Analysis of an Idealized Modern Wingsuit

Maria E. Ferguson

*Washington University in St. Louis, St. Louis, MO 63130*

**The modern wingsuit has been the subject of few scientific studies to date, and the prevailing design process remains the dangerous "guess-and-check" method. This study employed the commercial flow solver ANSYS Fluent to solve the steady Reynolds Averaged Navier-Stokes equations with turbulence models. The computational fluid dynamics (CFD) results provided information on the flow about a wingsuit designed with an airfoil cross section and large planform. The CFD simulation was performed using the Spalart-Allmaras turbulence model for the 3D wingsuit case and the k-kl-ω Transition model for the 2D airfoil case. Although the lack of experimental data available on wingsuit flight makes true validation difficult, the results of the 3D case were analyzed and compared to the 2D case, which was validated against data from the airfoil/wing management software Profili 2.0. The chosen airfoil had a stall angle of 13° and the wingsuit reached a stall angle of 48°, which appears higher than the actual effective angle of attack due to induced drag. This preliminary data indicates that the wingsuit as designed shows promise and could likely perform well under typical wingsuit flying conditions.**

## Nomenclature

| | | |
|---|---|---|
| $AR$ | = | aspect ratio, $AR = b^2/S$ |
| $a$ | = | slope of lift vs. angle of attack curve for a wing, $a = \frac{dC_L}{d\alpha}$ |
| $a_0$ | = | slope of lift vs. angle of attack curve for an airfoil |
| $\alpha$ | = | (geometric) angle of attack |
| $\alpha_i$ | = | induced angle of attack for a wing |
| $\alpha_{eff}$ | = | effective angle of attack for a wing, $\alpha_{eff} = \alpha - \alpha_i$ |
| $b$ | = | wingsuit span |
| $c$ | = | chord length |
| $C_D$ | = | drag coefficient |
| $C_L$ | = | lift coefficient |
| $C_m$ | = | momentum coefficient, or pitching moment |
| $C_p$ | = | pressure coefficient |
| $l$ | = | wingsuit length |
| $Re$ | = | Reynolds number |
| $S$ | = | planform area |

## I.    Introduction

Unlike a hang glider, jet pack, or small plane, the wingsuit avoids excessive apparatus or motors and allows the flyer to glide on his own power. Made of flexible, durable parachute fabric that inflates while in flight, wingsuits connect the limbs to create a wing with as much lift as possible given the limitations of the human body. The modern wingsuit has only been in existence since the 1990s [1], and although academics and manufacturers have begun to take a more scientific approach to wingsuit design, few truly rigorous analyses have been completed thus far. The lack of information on wingsuit aerodynamics puts designers and flyers at a dangerous disadvantage, but computational fluid dynamics (CFD) approaches provide risk-free information prior to the experimental trial stage.

The first step of creating a computer simulation of a wingsuit in flight is to generate the geometry of the wingsuit itself. Due in part to issues of intellectual property, along with the flexible nature of the wingsuit, it is

difficult to generate a geometry that exactly matches a commercial wingsuit. In addition, computational limitations require that for the present, the wingsuit must be assumed rigid. The project was therefore approached in an idealized fashion: at a certain instant in time, the wingsuit has a certain shape, and the rigid geometry reflects that shape at that moment. Furthermore, the ideal cross section for a wingsuit is an airfoil, so although the contours of the human body and the flexible fabric make that ideal unattainable, the cross section was assumed to be an airfoil. The idealized scenario lended itself to a comparison of the 2D results for the chosen airfoil cross section and the 3D results for the wingsuit geometry, since theoretical analyses already exist to compare a wing and its cross section. In addition, although there is no experimental data readily available for wingsuits, the airfoil/wing management software Profili 2.0 could be used to generate lift and drag data, which could then be used to validate the 2D airfoil case.

In 2D, the angle of attack of the air coming toward the leading edge of the airfoil is the angle of attack that the airfoil experiences. In wing theory, however, the airfoil cross sections in the wing experience an induced drag caused by downwash, a phenomenon where a small velocity component points downward toward the wing upper surface [2]. This leads to an induced angle of attack, which must be subtracted from the geometric angle of attack to obtain the effective angle of attack (the term "angle of attack" in the following text and plots shall indicate the geometric angle of attack unless specified otherwise). To obtain a general idea of how the effective angle of attack compares to the angle of attack set in the boundary condition, it can be calculated using $\alpha_{eff} = \alpha - \alpha_i$ (Equation 5.1 [2]). The induced angle of attack is easily calculated by assuming an elliptic wing. This is a large assumption, but the motivation is to observe a trend rather than obtain exact values, so it is sufficient as an approximation. Equation 5-43 [2] may be used to find $\alpha_i$:

$$\alpha_i = \frac{C_L}{\pi AR}$$

When the plot of lift coefficient vs. alpha of a 2D airfoil is compared to that of a 3D wing, it is expected that the 3D curve reach a higher angle of attack before stall and have a somewhat similar slope, according to the relation given in Equation 5-70 [2]:

$$\frac{dC_L}{d\alpha} = a = \frac{a_0}{1 + \frac{a_0}{\pi AR}(1 + \tau)}$$

The value of $\tau$ varies for a general wing planform, and $\tau = 0$ for an elliptic wing.

## II.    Geometry

Due to the flexible nature of the wingsuit, it is all but impossible to pinpoint its exact geometry in flight. The geometry was designed as an idealized approximation of the planform and cross section of suits currently on the market. The human body, including head, hands, feet, and body contours was excluded from the geometry, as was the parachute pack that typically rests like a backpack over the flyer's back.

Since the design was meant to reflect the ideal, the wingsuit was created with an airfoil cross section. The particular 2D airfoil cross section was chosen for its thickness and high camber, along with its lack of a large cavity in the undercamber. That is, the underside of the airfoil had a large curve relative to its chord line. The airfoil was also chosen for its lift coefficient, which was relatively high due to the camber.



**Figure 1: Wingsuit Planform**

The 3D geometry was created using Autodesk Inventor 2016 by connecting a center airfoil cross section to a smaller airfoil cross section on the wing edge. The resulting wingsuit had an airfoil cross section at any section cut, except for the very outer edges, where the airfoil cross section was at an angle parallel to the edge. The edges on the lower half of the suit, near the legs, were unrealistically thin due to the constraints of the CAD software. The thin areas are visible as the triangular portions on the lower left and right in Figure 1. The wingspan of the suit was designed to be 1.72 m and the height was 1.81 m so that it could accommodate a typical human body.
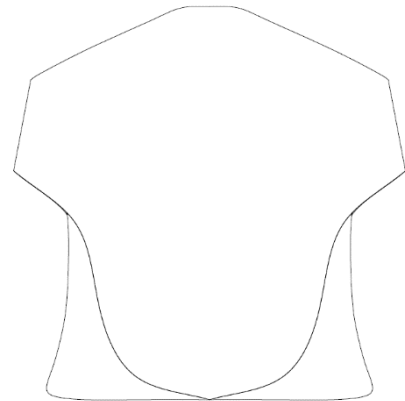
Some suits have cutouts, making a forward wing on the arms and another wing between the legs. Others stretch the fabric such that the forward wing reaches all the way to the legs, as shown in Figure 1. The planform was created in imitation of the relatively large aspect ratio suit designed for more experienced flyers.

## III.    Mesh Generation in ICEM

The 2D mesh for the airfoil validation case was created in the ANSYS meshing software ICEM in a C-Mesh with a 25 m far field and an airfoil chord length of 1 m, as shown in Figure 2. The final mesh after refinement had approximately 100,000 elements, with a finer grid near the airfoil and in its wake. A more detailed view of the geometry is shown in Figure 3.
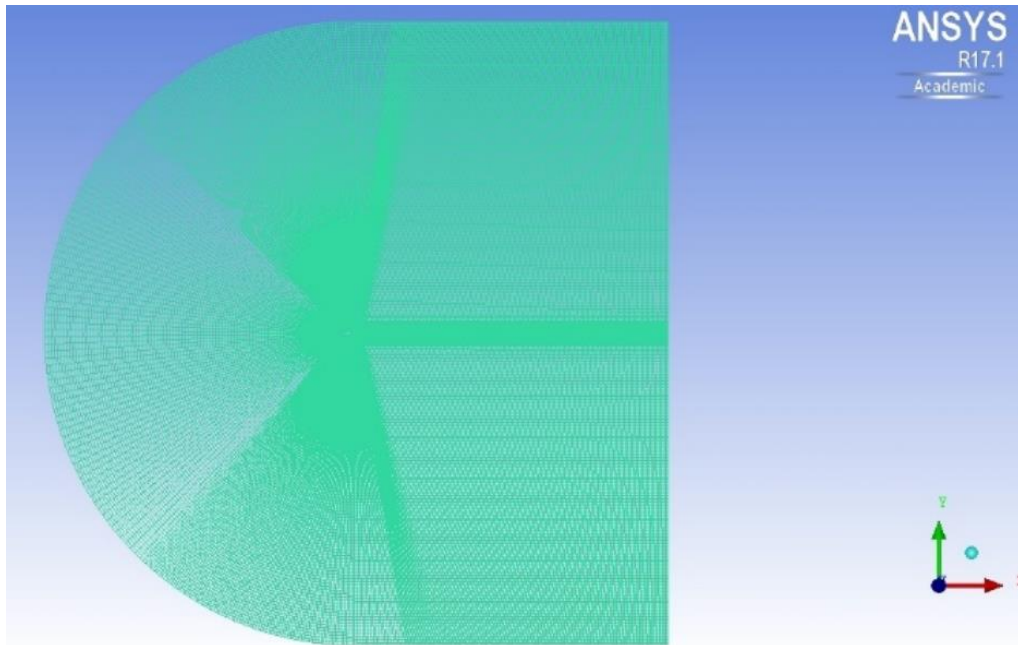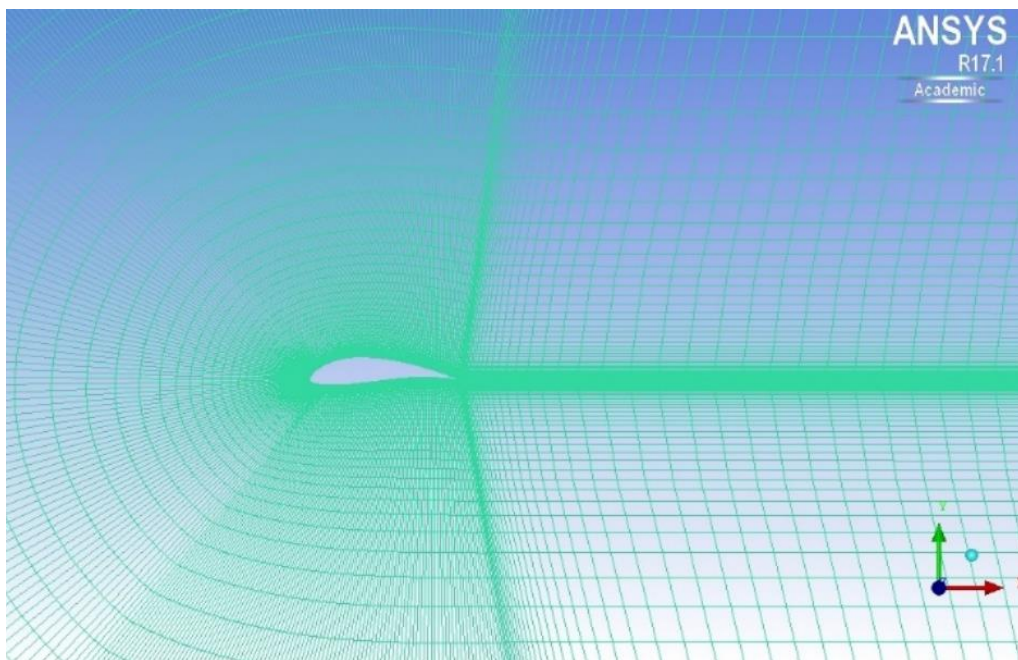


**Figure 2: C-Mesh with 25 m far field**



**Figure 3: C-Mesh near airfoil**

The 3D mesh was also created in ICEM and had a far field in the shape of an elliptical spheroid with major axis 60 m, minor axis 30 m, width 12 m, and a symmetry plane that cut through the middle of the wingsuit geometry. Near the wingsuit, a density region was created as shown in Figure 4. The final mesh had approximately 2.4 million elements.
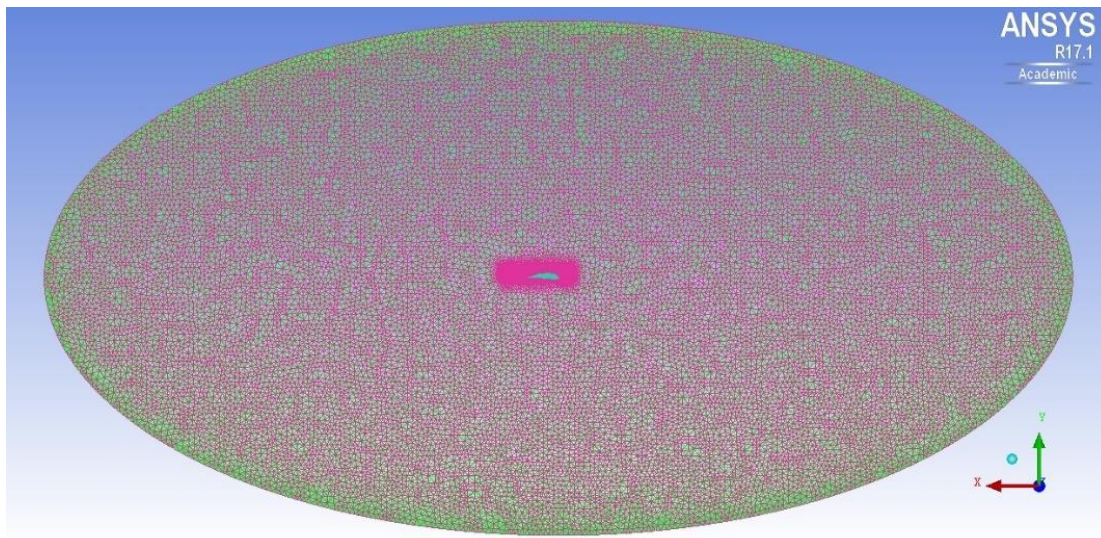


**Figure 4: 2.4 million element wingsuit mesh**

Since there was no experimental or literature values for the wingsuit, it was of vital importance to prove grid independence—that is, to show that the numerical results were not dependent on the mesh and that a finer mesh would yield the same results as the coarser mesh. The finer mesh was generated with the same geometry and far field, but with a smaller global element size and three density regions with increasing density toward the center instead of just one. This mesh had approximately 7.4 million elements.
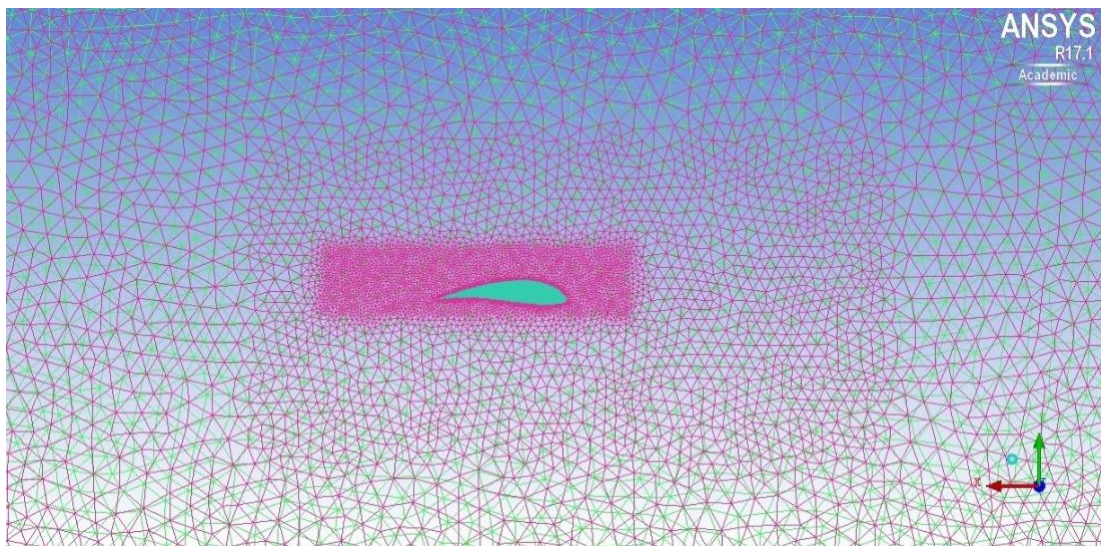


**Figure 5: 7.4 million element wingsuit mesh with density regions**

## IV.     Numerical Setup in ANSYS Fluent

The 2D airfoil case was run in a pressure-based, viscous, incompressible solver using the Transition k-kl-ω turbulence model. The entire geometry was scaled down by a factor of 0.1 to reduce the chord length from 1 m to 0.1 m and reduce the Reynold's number to a value that could be compared to literature values. The semi-circle in

front of the leading edge of the airfoil in Figure 2 was considered a velocity inlet with a magnitude of 45 m/s, which is a reasonable value for a wingsuit mid-flight and provides the best glide ratio at a comfortable speed [3]. The rear line was considered a pressure outlet.

The SIMPLE solution scheme with Second Order Upwind momentum was used. The case was run for an angle of attack from 0 to 14° in steps of two degrees until the lift and drag coefficients for each case oscillated by less than one percent.

The 3D wingsuit case was run in a pressure-based, viscous, solver using the Spalart-Allmaras turbulence model with air density set to ideal gas. The plane cutting the geometry in half was set as a symmetry plane, and the far field was set as a pressure far field. The Mach number was set to 0.132, which corresponds to a velocity of 45 m/s. The area was set to 1 m$^2$, which would produce nondimensionalized lift and drag coefficients that would later be multiplied by the planform half area, 1.25 m$^2$, to obtain values for the lift and drag coefficients. The length was set to 1.84 m due to a slight measurement error (the actual length was 1.81 m). The momentum coefficient was calculated about the quarter chord, at 0.46 m along the x-direction.

The SIMPLE solution scheme with Second Order Upwind momentum was used for the 3D case. The case was run for an angle of attack from 0 to 50° in steps of two degrees until the lift and drag coefficients for each case oscillated by less than one percent.

## V.    Numerical Results for 2D Airfoil and 3D Wingsuit

**2D Airfoil Results**

The Reynolds number for the 2D case was $2.4 \times 10^5$ assuming air properties at 10,000 ft and a chord length of 10 cm. The software Profili 2.0 provides airfoil data up to the angle of stall, and this data was compared to the data obtained from Fluent using the k-kl-ω model as shown in Figure 6 and Figure 7. The greatest error was at 0° angle of attack, with the Fluent data 19% and 45% lower than the Profili data for lift and drag coefficient, respectively. Otherwise, the data matched well and showed stall after 12° as predicted by Profili. The success of the 2D validation case provides greater confidence in the 3D case to come.
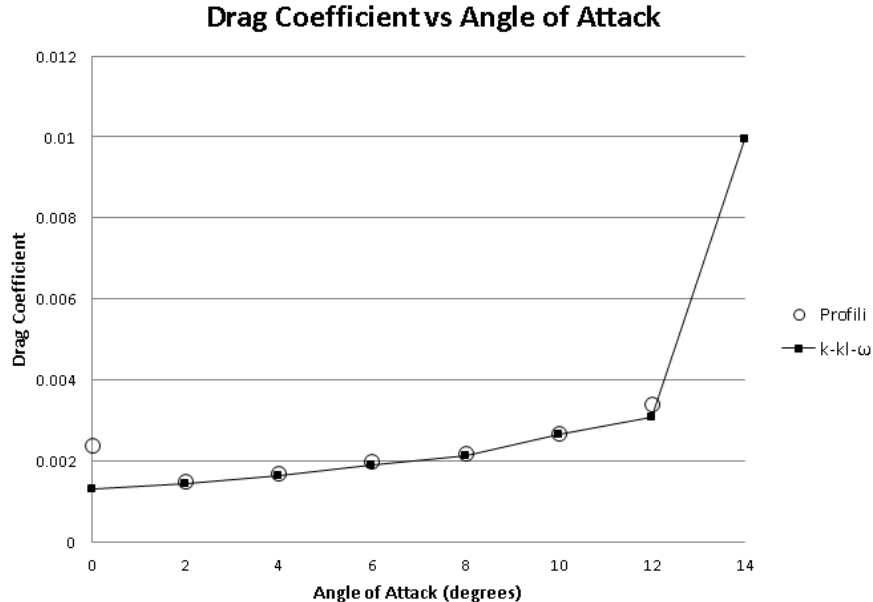


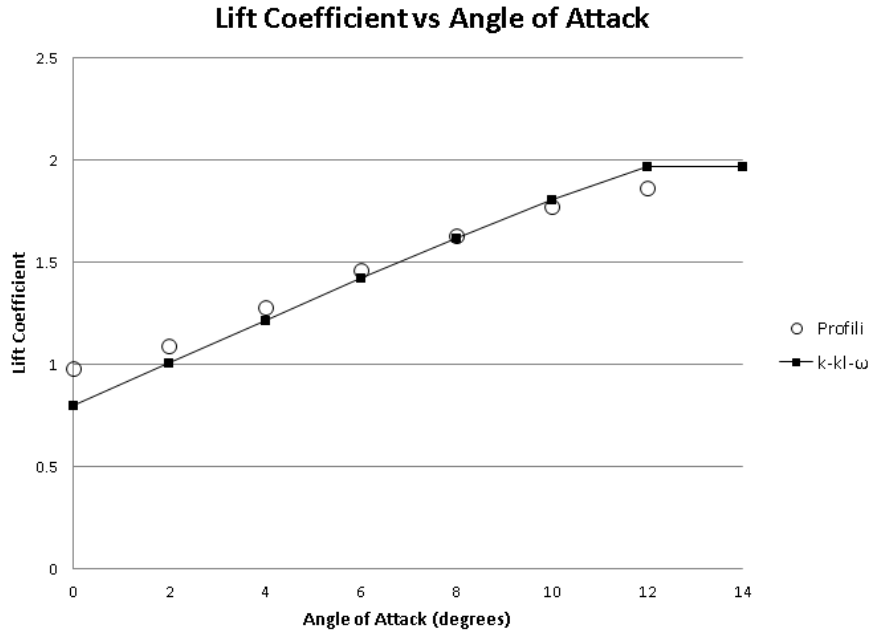**Figure 6: Drag coefficient literature and numerical values**

## Lift Coefficient vs Angle of Attack

Figure showing Lift Coefficient (y-axis, 0 to 2.5) vs Angle of Attack (degrees) (x-axis, 0 to 14), with two series: Profili (open circles) and k-kl-ω (filled squares).

**Figure 7: Lift coefficient literature and numerical values**

### 3D Wingsuit Results

The 3D cases converged within several thousand iterations until about 26° angle of attack, after which point the convergence history showed some oscillation. By 46° angle of attack, the cases were run for tens of thousands of iterations, but eventually the oscillations became small enough to consider the solution converged. The lift increased linearly until 48° angle of attack, at which point a large drop in lift became evident. Thus, 48° was considered the stall angle for the wingsuit. The coefficients of lift, drag, and momentum were multiplied by the wingsuit area to obtain the results shown in Figure 8.
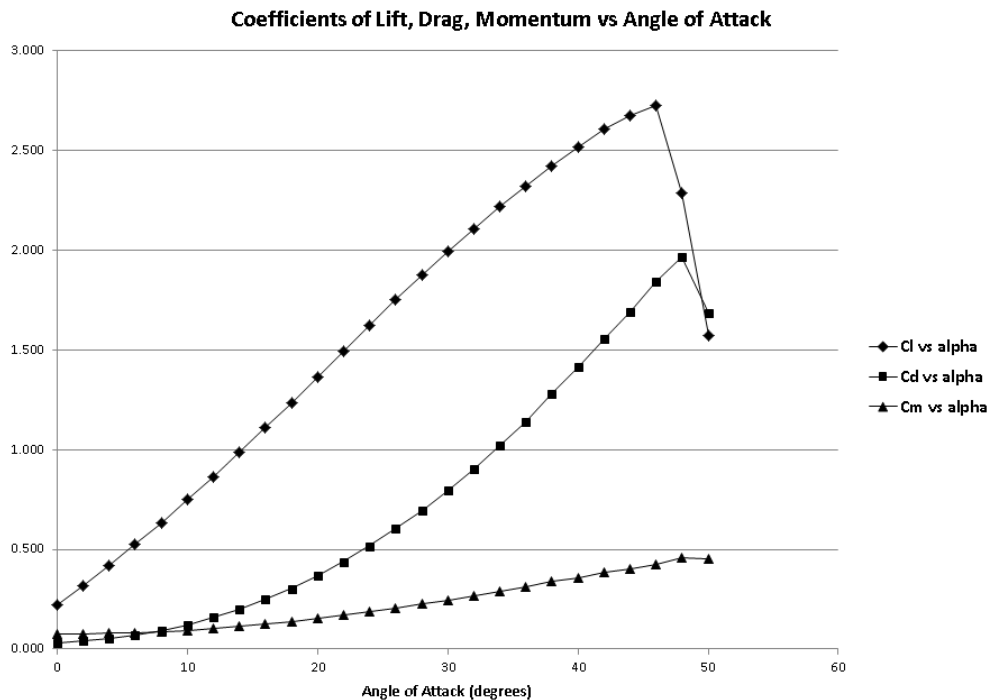
## Coefficients of Lift, Drag, Momentum vs Angle of Attack

Figure showing Coefficients (y-axis, 0.000 to 3.000) vs Angle of Attack (degrees) (x-axis, 0 to 60), with three series: Cl vs alpha (diamonds), Cd vs alpha (squares), and Cm vs alpha (triangles).

**Figure 8: Coefficients of lift, drag, and momentum vs. angle of attack**

The quality of these results was evaluated in two ways: testing for mesh independence and comparing the 3D wingsuit curves to the 2D airfoil curves. The mesh independence test at 6 and 12° angles of attack produced the same results for $C_D$, $C_L$, and $C_m$ with less than 1% error, proving that the results were independent of the mesh.

When the 3D lift curve was compared to the 2D curve, a surprisingly large number of angles of attack was obtained before reaching stall at 48°, and the 3D slope was lower than expected based on Equation 5-70 [2]. Based on an airfoil slope of 0.0987, the expected elliptic wing slope would be 0.0975. Although the value of $\tau$ for this unusual geometry is unknown, $\tau$ usually ranges from 0.05 to 0.25, which gives the potential predicted wing slope a range of 0.0972 to 0.0975. The slope obtained from CFD was 0.0577, as shown in Figure 9.
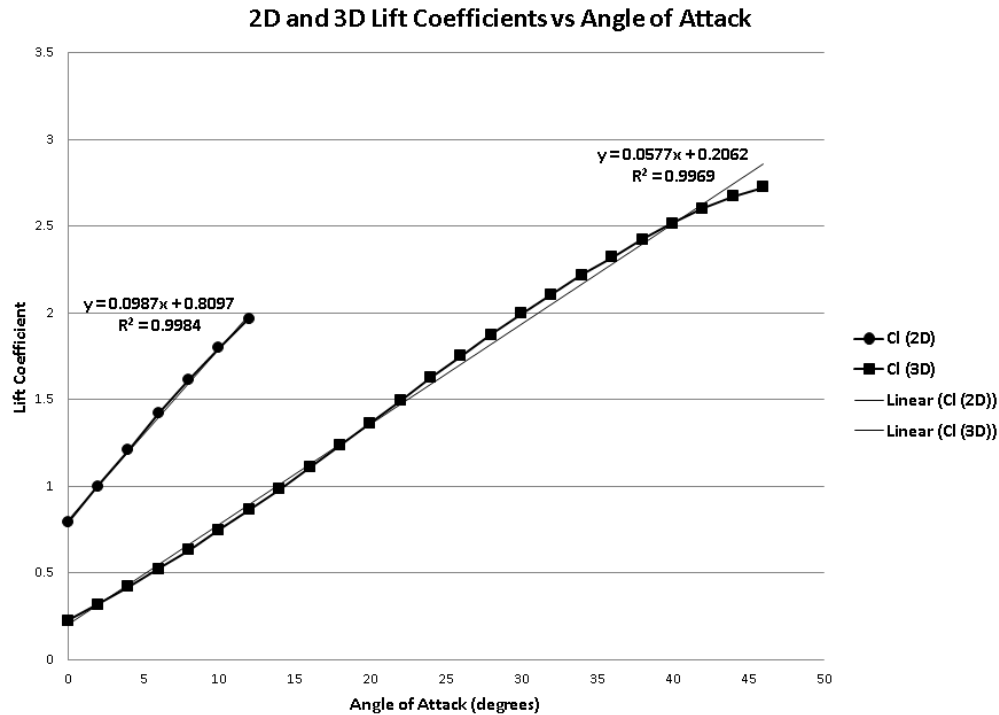


**Figure 9: Comparison of 2D airfoil and 3D wingsuit lift coefficients vs. geometric angle of attack with linear curve fits**

The discrepancy between the predicted slope $a$ and that obtained by CFD can be partially explained by the phenomenon of the effective angle of attack. In fact, although the effective angle of attack given by Equations 5.43 and 5.1 [2] assumes an elliptic wing and is therefore highly approximate, it demonstrates that the effective angle of attack is smaller than the geometric angle of attack. The effective angle of stall is thus between 27 and 32° rather than 48°. The induced angle of attack is large, and would be even larger if it could be calculated without the elliptic assumption. Plotting the 3D CFD results against the effective angle of attack rather than the geometric one brings the slope much closer to the expected value, with a value of 0.0964 as shown in Figure 10. Again, this result comes about from a very large assumption and should not be taken as numerically accurate, but the fact that the data shifts in the correct direction and comes closer to the expectation is reassuring.
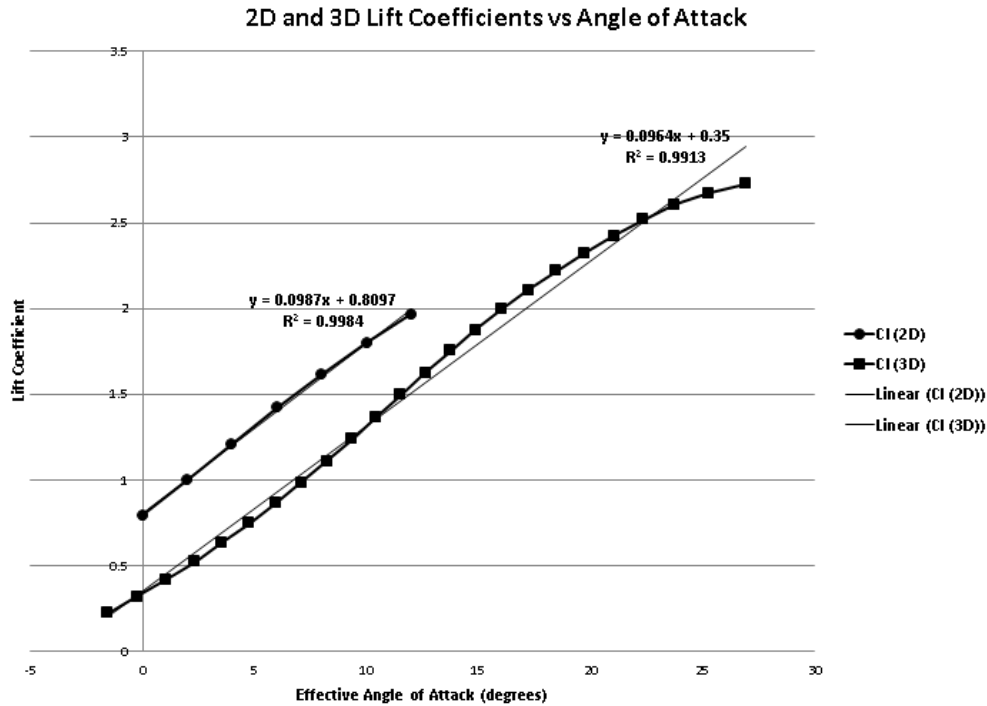
**Figure 10: Comparison of 2D airfoil and 3D wingsuit lift coefficients vs. effective angle of attack with linear curve fits**

Knowing more about the airflow as the angle of attack increases is useful in understanding how the wingsuit would behave in actual flight conditions. The 2D pressure plots for various cross sections of the wingsuit were generated with the sectional views as shown in Figure 11.
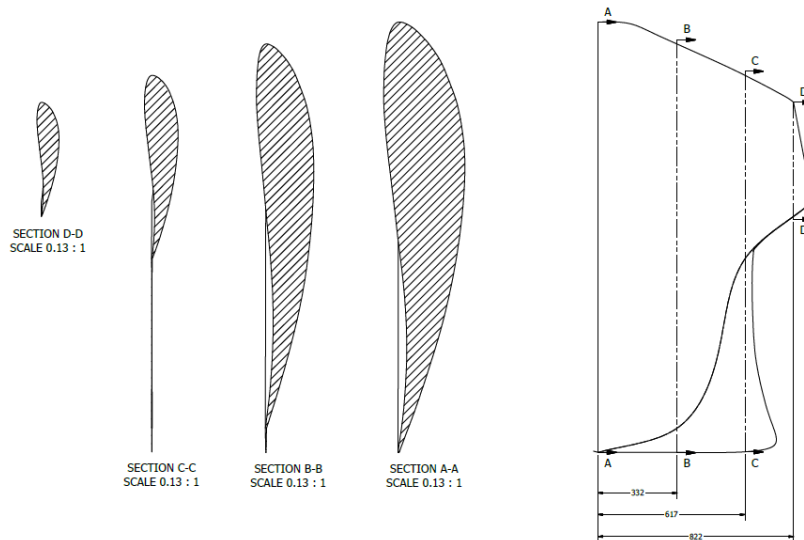


**Figure 11: 2D cross sections and locations A through D at z = 0.000, 0.332, 0.617, and 0.822 m from center line**

The pressure plots are given in the following four figures. For each cross section, the pressure coefficient is plotted for 8, 16, 24, 32, 40, and 48° angles of attack.
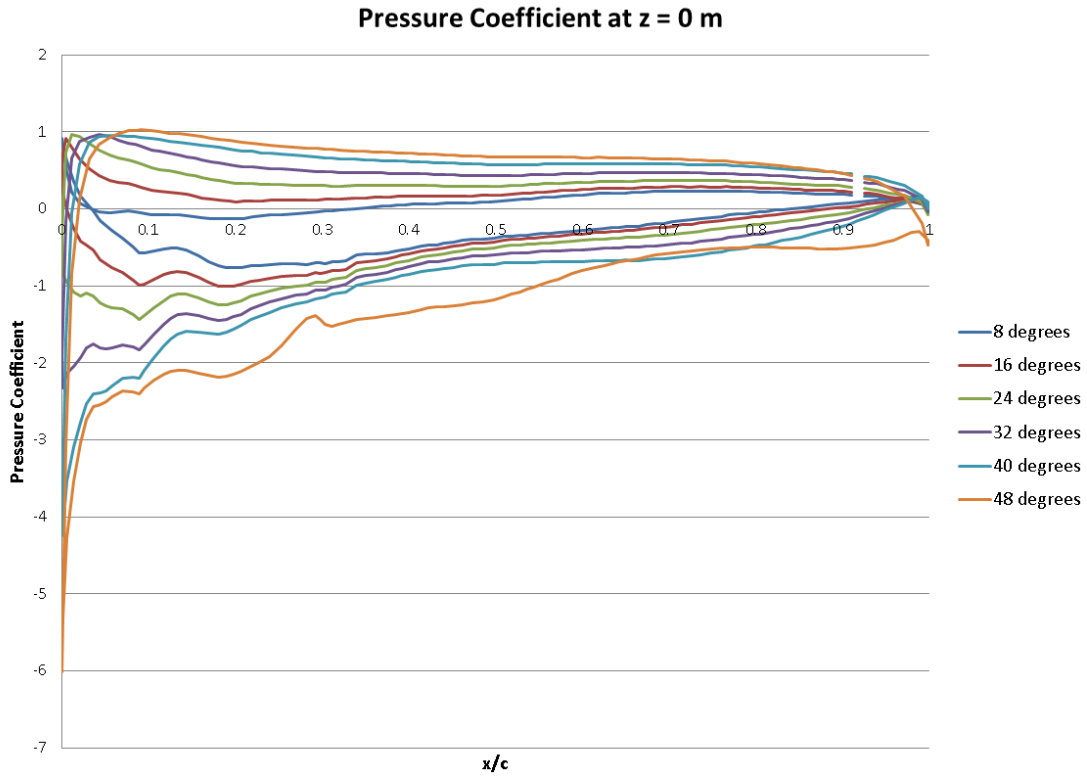
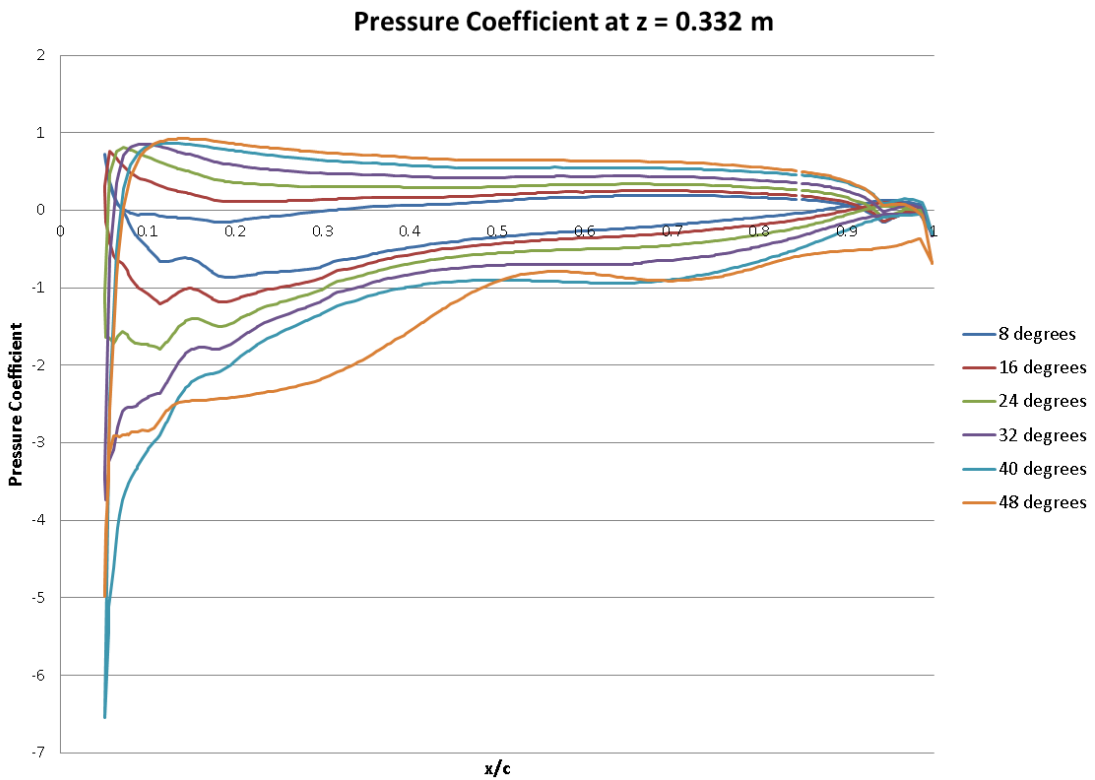**Figure 12: Pressure coefficient vs. x/c for 8, 16, 24, 32, 40, and 48° at z = 0.000 m from centerline**



**Figure 13: Pressure coefficient vs. x/c for 8, 16, 24, 32, 40, and 48° at z = 0.332 m from centerline**
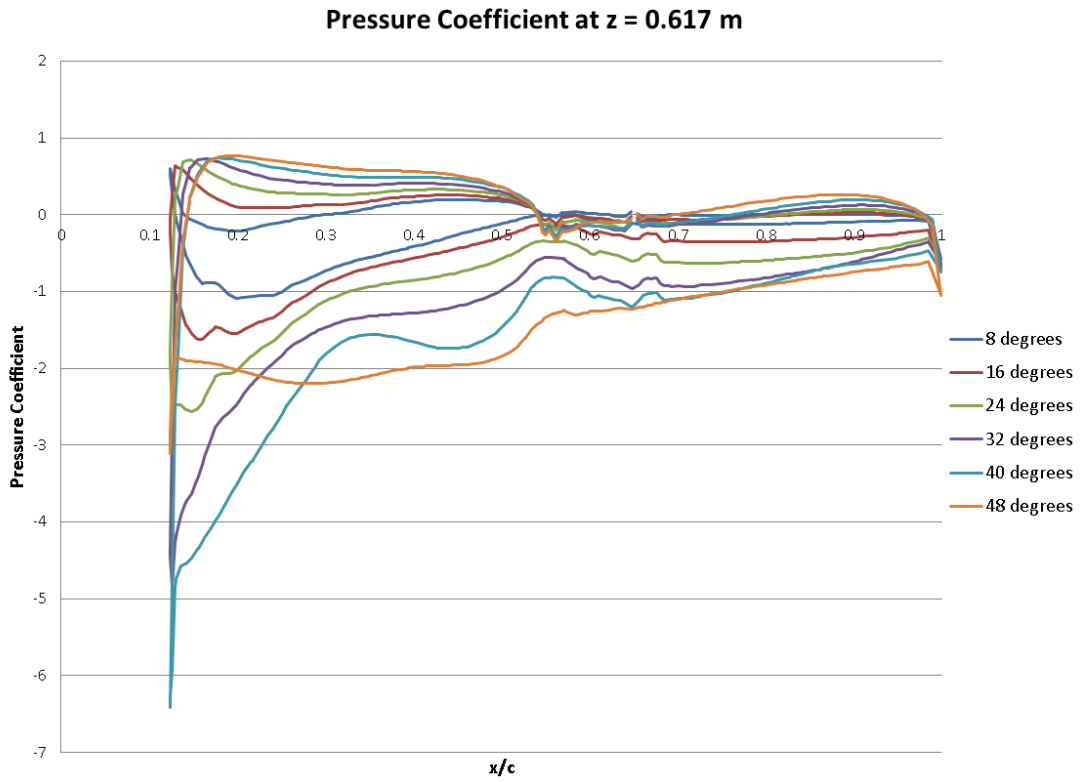
**Figure 15: Pressure coefficient vs. x/c for 8, 16, 24, 32, 40, and 48° at z = 0.617 m from centerline**
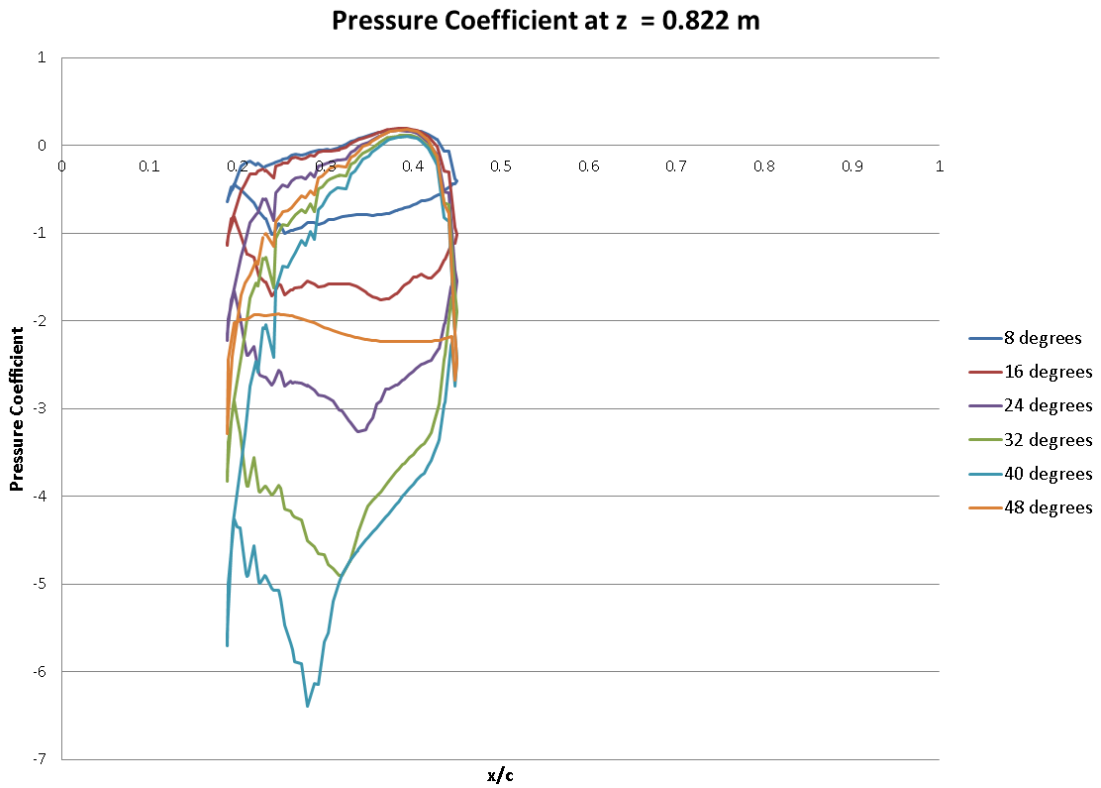


**Figure 14: Pressure coefficient vs. x/c for 8, 16, 24, 32, 40, and 48° at z = 0.822 m from centerline**

Finally, the flow can also be visualized in 3D. In Figure 16, the pressure contours on the wingsuit are visible as well as the velocity streamlines, which demonstrate the vortical motion typical of the edges of a wing. The edges of the wing also show lower pressure zones, and there is higher pressure on the back side of the airfoil than on the front side.
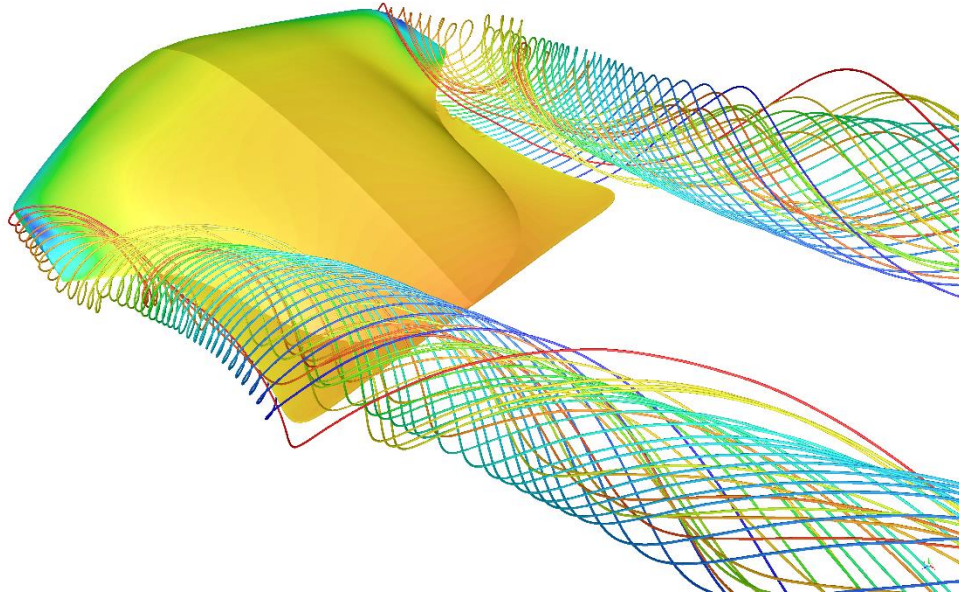


**Figure 16: 3D wingsuit at 45 m/s and 32° angle of attack with surface pressure contours and velocity streamlines from wing edges**

Comparing the flow at a 12° angle of attack to the flow at 32°, we see that the vortical motion increases in size and turbulence as the angle of attack increases. This is evident in Figure 17 and Figure 18 below.
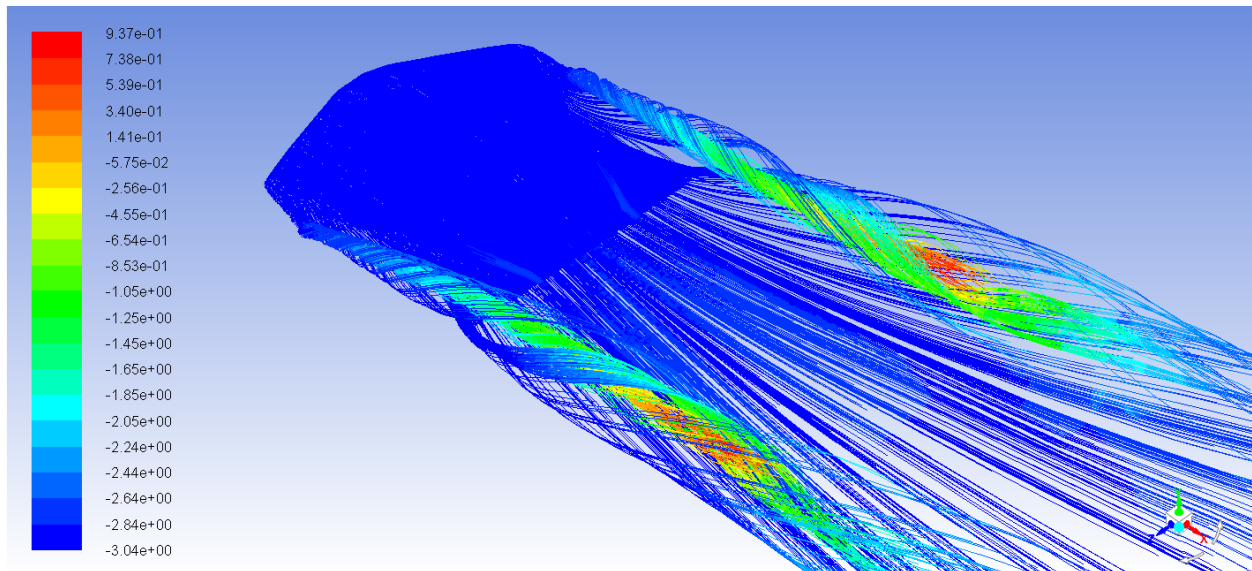


**Figure 17: 3D wingsuit at 45 m/s and 12° angle of attack with streamlines colored by Modified Turbulent Viscosity**
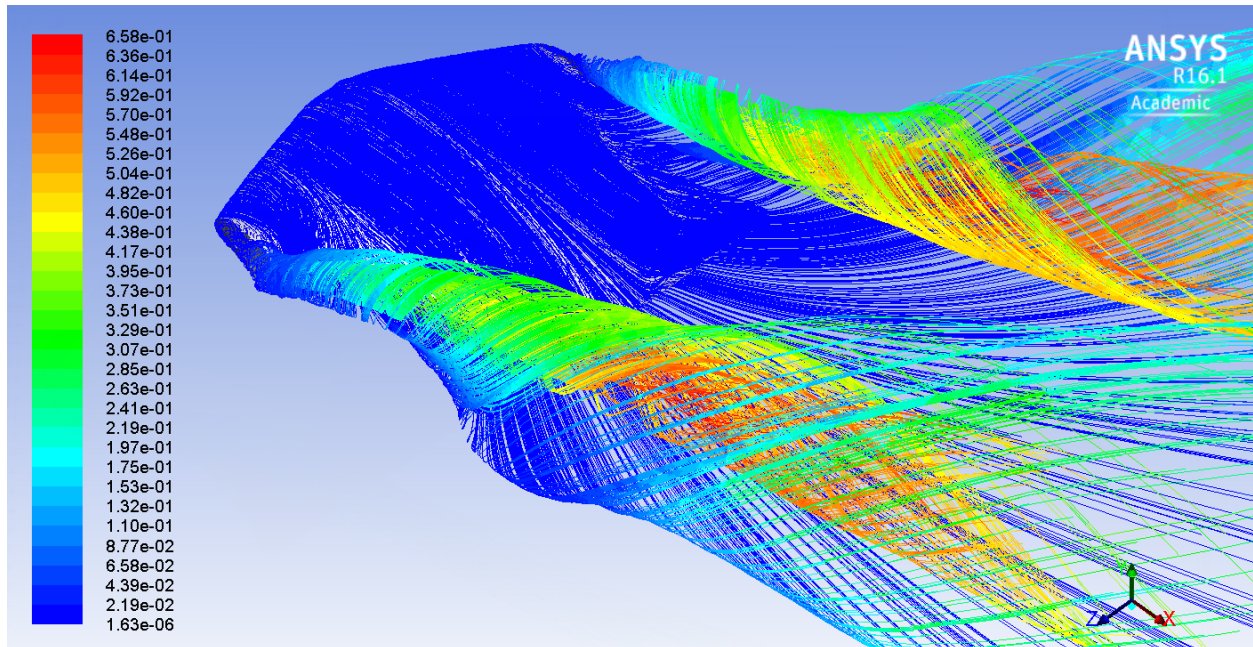
**Figure 18: 3D wingsuit at 45 m/s and 32° angle of attack with streamlines colored by Modified Turbulent Viscosity**

## VI.     Conclusions and Future Work

One of the major problems of research related to wingsuits is the lack of information available, but each research project helps lay groundwork for the next project, and eventually there will be a more solid foundation to build upon. This study turned the lack of information on wingsuit geometry into an opportunity to examine the behavior of an ideal wingsuit with an airfoil cross section. Future work might include more realistic geometries that take into account human features, and perhaps a fluctuating geometry that simulates the motion of the flexible wingsuit fabric.

Using pressure coefficient data and velocity streamlines, more detail should be acquired regarding the changes in the behavior of the airflow about the wingsuit as the angle of attack is increased. Although the validation techniques for the 3D case seemed to indicate that the results of this simulation were reasonable, the values should be compared to experimental data if possible. It might also be worthwhile to run the same cases with different turbulence models to gain more confidence in the simulation results.

## References

[1] W. S. Weed, "The Flight of the Bird Men," 18 June 2003. [Online]. Available: http://www.popsci.com/military-aviation-space/article/2003-06/flight-bird-men.

[2] J. John D. Anderson, Fundamenals of Aerodynamics, New York, NY: McGraw Hill, 2011.

[3] G. Robson and R. D'Andrea, "Longitudinal Stability Analysis of a Jet-Powered Wingsuit," *AIAA Guidance, Navigation, and Control Conference,* 2010.